Eight New Quasar Lenses from the Sloan Digital Sky Survey Quasar Lens Search

Issha Kayo[1,2,3], Naohisa Inada[4], Masamune Oguri[5,6], Tomoki Morokuma[3,5], Patrick B. Hall[7], Christopher S. Kochanek[8], Donald P. Schneider[9]

ABSTRACT

We report the discovery and confirmation of eight new two-image lensed quasars by the Sloan Digital Sky Survey (SDSS) Quasar Lens Search. The lenses are SDSS J0904+1512 (image separation $\theta = 1\farcs13$, source redshift $z_s = 1.826$), SDSS J1054+2733 ($\theta = 1\farcs27$, $z_s = 1.452$), SDSS J1055+4628 ($\theta = 1\farcs15$, $z_s = 1.249$), SDSS J1131+1915 ($\theta = 1\farcs46$, $z_s = 2.915$), SDSS J1304+2001 ($\theta = 1\farcs87$, $z_s = 2.175$), SDSS J1349+1227 ($\theta = 3\farcs00$, $z_s = 1.722$), SDSS J1455+1447 ($\theta = 1\farcs73$, $z_s = 1.424$), and SDSS J1620+1203 ($\theta = 2\farcs77$, $z_s = 1.158$). Three of them, SDSS J1055+4628, SDSS J1455+1447, and SDSS J1620+1203, satisfy the criteria for constructing our statistical sample for studying the cosmological model. Based on galactic absorption lines of the lens galaxies, we also derive lens redshifts of $z_l = 0.398$ and $z_l = 0.513$ for SDSS J1620+1203 and the previously discovered lens SDSS J0746+4403, respectively.

Subject headings: gravitational lensing: strong — quasars: general

[1]Institute for the Physics and Mathematics of the Universe, University of Tokyo, 5-1-5 Kashiwanoha, Chiba 277-8582, Japan

[2]Institute of Cosmology and Gravitation, University of Portsmouth, Burnaby Road, Portsmouth, PO1 3FX, UK

[3]Research Fellow of the Japan Society for the Promotion of Science

[4]Cosmic Radiation Laboratory, RIKEN, 2-1 Hirosawa, Wako, Saitama 351-0198, Japan.

[5]National Astronomical Observatory, Osawa, Mitaka, Tokyo 181-8588, Japan

[6]Kavli Institute for Particle Astrophysics and Cosmology, Stanford University, 2575 Sand Hill Road, Menlo Park, CA 94025, USA

[7]Department of Physics and Astronomy, York University, 4700 Keele Street, Toronto, Ontario M3J 1P3, Canada

[8]Department of Astronomy, The Ohio State University, 4055 McPherson Lab, 140 West 18th Avenue, Columbus, OH 43210, USA

[9]Department of Astronomy and Astrophysics, Pennsylvania State University, 525 Davey Laboratory, University Park, PA 16802, USA

1. Introduction

Gravitationally lensed quasars play important roles not only in investigating the physical properties of lens galaxies but also in extracting cosmological information and constraining the structure of quasar accretion disks (e.g., see Schneider et al. 2006; Kochanek 2006, for reviews). To use lensed quasars for these studies, it is important to construct large samples, especially for cosmological purposes. The Cosmic Lens All-Sky Survey (CLASS; Myers et al. 2003; Browne et al. 2003) is one of the largest, with 22 lenses drawn from a sample of $\sim 16,000$ radio sources, and has provided useful constraints on the evolution of galaxies and cosmology. We are performing a systematic lensed quasar survey, the Sloan Digital Sky Survey Quasar Lens Search (SQLS; Oguri et al. 2006; Inada et al. 2008), to construct a larger sample of lensed quasars in the optical. Thus far, we have discovered 28 lensed quasars (26 are galaxy-scale lenses and two are cluster-scale lenses) and rediscovered 11 known lenses (e.g., Oguri et al. 2008b; Inada et al. 2009a, and references therein). Our current sample is now large enough for the statistical errors on cosmological parameters to be comparable to the present level of the systematic uncertainties (Oguri et al. 2008a). Larger samples of lensed quasars also allow an increasing level of "self-calibration" to constrain many of these uncertainties, particularly the velocity dispersion function of the lens galaxies and its evolution as one of the largest contributors to these systematic uncertainties (e.g., Choi et al. 2007; Matsumoto & Futamase 2008; Chae 2008).

In this paper, we report the discovery of new eight galaxy-scale lenses done by early in 2009, bringing our total sample to 47[1]. We briefly describe the selection of lens candidates from the Sloan Digital Sky Survey (SDSS; York et al. 2000) in the following section, and then present the imaging and spectroscopic observations needed to confirm these candidates in Section 3. Simple mass models of the eight lenses are made in Section 4 to see whether the lensing interpretation is reasonable. Throughout the paper, we assume a standard cosmological model with matter density $\Omega_M = 0.26$, cosmological constant $\Omega_\Lambda = 0.74$, and Hubble constant $H_0 = 72 \mathrm{km\ s^{-1} Mpc^{-1}}$.

2. SDSS Data and Selection of Candidates

The SDSS-I and SDSS-II Sloan Legacy Surveys are photometric and spectroscopic surveys (Fukugita et al. 1996; Gunn et al. 1998; Lupton et al. 1999; Stoughton et al. 2002; Blanton et al. 2003; Tucker et al. 2006) covering a quarter of the all sky, using a dedicated

---

[1] Visit http://www-utap.phys.s.u-tokyo.ac.jp/~sdss/sqls/ for a list of lensed quasars in the SQLS.

telescope (Gunn et al. 2006) at the Apache Point Observatory in New Mexico, USA. The imaging data were processed by the photometric pipeline (Lupton et al. 2001) and carefully calibrated (Hogg et al. 2001; Smith et al. 2002; Pier et al. 2003; Ivezić et al. 2004). The spectroscopic quasar targets were selected from the imaging data according to the algorithm described by Richards et al. (2002) and cataloged in Schneider et al. (2007) and D. P. Schneider et al. (2010, in preparation). All the SDSS data are publicly available in the final Data Release 7 (Abazajian et al. 2009).

From the spectroscopically confirmed quasar catalogs we select candidates for lensed quasars using two different methods based on morphologies (morphological selection) and color (color selection). The details of the two selection methods are found in Inada et al. (2008) and Oguri et al. (2006). Morphological selection is used to find lenses with small image separations, $\lesssim 2\rlap{.}''5$, which are not deblended by the SDSS pipeline, and color selection is for lenses with larger separations. Of the eight systems reported in this paper, five systems (SDSS J0904+1512, SDSS J1054+2733, SDSS J1055+4628, SDSS J1131+1915, and SDSS J1455+1447) were morphologically selected, and three (SDSS J1304+2001, SDSS J1349+1227, and SDSS J1620+1203) were color selected. The finding charts for the systems are shown in Figure 1, and the SDSS properties of the systems are listed in Table 1. Three systems, SDSS J1055+4628, SDSS J1455+1447, and SDSS J1620+1203, satisfy the criteria for our statistical sample used for cosmological studies (source redshift $0.6 < z_s < 2.2$, image magnitude $i < 19.1$, image separation $1'' < \theta < 20''$, flux ratio between images ΔI or $\Delta i < 1.25$; see Inada et al. 2008; Oguri et al. 2008a; Inada et al. 2009a, for the complete description).

3. Additional Imaging and Spectroscopy

The imaging observations for these lenses were performed using four instruments on the University of Hawaii 2.2 m telescope (UH88): the Tektronix 2048x2048 CCD camera (Tek2k; the pixel size is $0\rlap{.}''2195$ pixel^{-1}), the UH8k wide-field imager (UH8k; $0\rlap{.}''235$ pixel^{-1}), the Orthogonal Parallel Transfer Imaging Camera (OPTIC; $0\rlap{.}''1374$ pixel^{-1}), and the Quick Infrared Camera (QUIRC; $0\rlap{.}''189$ pixel^{-1}). The spectroscopic data and some images were taken with the Faint Object Camera and Spectrograph (FOCAS; Kashikawa et al. 2002) on the Subaru telescope. The FOCAS data were binned 2×2 on the detector leading to a spatial resolution of $0\rlap{.}''208$ pixel^{-1}. The spectral resolution is $R \sim 400 - 500$. Tables 2 and 3 summarize the observations.

We analyzed the imaging data using GALFIT (Peng et al. 2002). First we fit each system with two stellar components using stars near the systems as point-spread function (PSF) templates. There remained significant extended residuals between the point sources

after subtracting the best-fit model for all systems. We then added a galaxy modeled by a Sérsic profile to the fit and found virtually no residuals. In the left panels of Figure 2, we show the original I-band images (R-band image for SDSS J1055+4628). Most of the signal in the images arises from two point-like objects, labeled "A" and "B". In the right panels we show the residuals, labeled "G1" or "G2", after subtracting the two best-fit PSFs. The astrometry and photometry of the components are listed in Table 4, and the best-fit Sérsic parameters are shown in Table 5. The differences in the relative positions of these components between bands are below $0\rlap{.}''05$ for the stellar components and $0\rlap{.}''2$ for the extended components.

The one-dimensional spectra of the stellar components were extracted using standard IRAF[2] tasks. The spectra shown in Figure 3 and the results of the imaging observations unambiguously confirm that the eight systems are gravitationally lensed systems. The shapes of the various emission lines and continua are almost perfectly identical between the two quasars of each system. The spectrum of the fainter quasar of SDSS J1620+1203 is contaminated with the relatively bright lens galaxy, and we clearly detect some galactic absorption lines of the lens galaxy. We conclude with comments on individual lens system.

SDSS J0904+1512. The I-band image shows that the lens galaxy is located near the brighter lens image, like HE1104-1805 (Wisotzki et al. 1993) or SDSS J1226-0006 (Inada et al. 2008), and a fit to the galaxy profile yields the Sérsic index of 4.1. When analyzing V- and R-band images, we fixed the galaxy profile to the I-band profile because the galaxy is too faint to fit the galaxy profile correctly. The image separation is $\theta = 1\rlap{.}''128 \pm 0\rlap{.}''007$, and the source redshift is $z_s = 1.826 \pm 0.002$. This lens system is not included in the SQLS statistical sample because of the large flux ratio between the quasar images ($\Delta I > 1.25$; Inada et al. 2008).

SDSS J1054+2733. The best-fit Sérsic index to the galaxy is 3.7 in the I-band, and the lens galaxy is likely to be early-type. For the R-band analysis, we fixed the galaxy profile to that from the I-band fit. Although there remain some residuals in the 2PSFs model of the V-band image, we could not fit the residuals well because of a lack of bright enough PSF templates to fit the weak residuals. The image separation is $\theta = 1\rlap{.}''269 \pm 0\rlap{.}''004$ and the source redshift is $z_s = 1.452 \pm 0.002$. This system is not included in the SQLS statistical sample because of the large flux ratio between the images.

---

[2]IRAF is distributed by the National Optical Astronomy Observatories, which are operated by the Association of Universities for Research in Astronomy, Inc., under cooperative agreement with the National Science Foundation.

SDSS J1055+4628. The FOCAS R-band image was used for astrometric measurements because it is the deepest. In addition to the two quasars (A and B) and the lens galaxy (G1 with a best-fit Sérsic index of 5.4), we also found two extended objects located $3\overset{''}{.}5$ to the north and $4''$ to the south of the system. The northern object has $R - I \sim 1.0$, which is similar to the lens galaxy G1 ($R - I = 0.87$), but the southern one is much bluer than the two galaxies. In the V-band image we could not find any galaxy components. The image separation is $\theta = 1\overset{''}{.}146 \pm 0\overset{''}{.}004$ and the source redshift is $z_s = 1.249 \pm 0.001$. This system satisfies our statistical sample criteria and is included in SQLS statistical sample from DR5 (N. Inada et al. 2010, in preparation).

SDSS J1131+1915. The lens galaxy was successfully fit in the I band image with the Sérsic profile (the best-fit index is 2.4), but the V-band residuals after subtracting two PSFs are faint and we could not estimate the parameters of the galaxy. We did not take R-band images. The image separation is $\theta = 1\overset{''}{.}462 \pm 0\overset{''}{.}007$ and the source redshift is $z_s = 2.915 \pm 0.001$. This system is not included in the SQLS statistical sample because the redshift is outside of our selection criteria ($z_s < 2.2$).

SDSS J1304+2001. We fit the images with two PSFs (A and B) and two Sérsic profiles (G1 and G2), and the best-fit Sérsic indices are 2.9 and 6.0, respectively. Galaxy G1 lies between the two quasars and galaxy G2 is located about $3\overset{''}{.}5$ to the south of G1. G1 and G2 have similar, red colors ($R - I = 0.7 \sim 1.0$ and $V - R = 0.8 \sim 0.9$), suggesting that they are probably associated with each other. The image separation is $\theta = 1\overset{''}{.}865 \pm 0\overset{''}{.}004$ and the source redshift is $z_s = 2.175 \pm 0.002$. This system is not included in the SQLS statistical sample because of the large flux ratio between the images.

SDSS J1349+1227. Although this system had been reported as a binary quasar in Hennawi et al. (2006), our new observations suggest that it is a gravitational lens rather than a binary quasar. We detected a lens galaxy very close to the fainter quasar component with a best-fit Sérsic index of 1.7. Because the galaxy is faint in the R- and V-bands, we fixed the galaxy parameters to the best-fit values from the I-band. The image separation is $\theta = 3\overset{''}{.}002 \pm 0\overset{''}{.}004$ and the source redshift is $z_s = 1.722 \pm 0.002$. This system is not included in the SQLS statistical sample because the flux ratio is slightly outside of our selection criteria (N. Inada et al. 2010, in preparation).

SDSS J1455+1447. We fit the I-band image with two PSFs and a galaxy, and the best-fit Sérsic index was 3.5. As in the case of SDSS J1349+1227, we fixed the galaxy profile in

R and V to the best-fit values from the I-band. The image separation is $\theta = 1\rlap{.}''727 \pm 0\rlap{.}''004$ and the source redshift is $z_s = 1.424 \pm 0.001$. This system will be included in the SQLS DR7 statistical sample (N. Inada et al. 2010, in preparation).

SDSS J1620+1203. The lens galaxy is bright and close to the faint quasar, and the spectral features of the galaxy are seen in the spectrum of the faint quasar. In fact, the fainter quasar image was classified as a galaxy in the SDSS due to the bright lens galaxy. Ca II H&K , Mg, and Na galactic absorption lines are observed, giving a lens galaxy redshift of $z_l = 0.398 \pm 0.001$. The image separation is $\theta = 2\rlap{.}''765 \pm 0\rlap{.}''011$ and the source redshift is $z_s = 1.158 \pm 0.002$. The best-fit Sérsic index of 6.62 ± 2.53 is larger than is expected (Blanton et al. 2005), but we do not take it seriously because of the large error. This system will be included in the SQLS DR7 statistical sample (N. Inada et al. 2010, in preparation).

4. Mass Modeling

We modeled all eight systems to see whether the lensing hypothesis is reasonable from the theoretical point of view. Because of the small number of observational constraints for two image lenses, we limited the model to a singular isothermal ellipsoid (SIE) without any external shear. This mass model has five parameters: the lens position, the Einstein radius R_E, ellipticity e, and position angle θ_e (measured east of north). If we fit the relative positions and the image flux ratio, these two image lenses provide only five constraints, so our model has no degrees of freedom and we can find a perfectly fitting model with $\chi^2 \sim 0$ as long as the model is reasonable. To find the best-fit mass models, we used the *glafic* software (M. Oguri, in preparation; version 1.0). We used the positions and I-band fluxes in Table 4. Only one lens galaxy was considered even if there are nearby galaxies that could appreciably affect the lens potentials, as in the case of SDSS J1055+4628 and SDSS J1304+2001. The resulting parameters are summarized in Table 6. As expected, the fitting was done with $\chi^2 \sim 0$ for all lens systems.

We estimated likely redshifts of the lens galaxies from the observed I-band magnitudes using the modified Faber–Jackson relation of Rusin et al. (2003). The estimated redshifts and the expected V- and R-band magnitudes at the redshifts are listed in Table 7. For SDSS J1620+1203 we list the spectroscopically confirmed redshift. Considering the scatter of the relation, ~ 0.5 mag, the predicted magnitudes agree well with the observations, except for SDSS J0904+1512 and SDSS J1349+1227. The lens galaxy of SDSS J0904+1512 is bright in the I-band, which makes the expected redshift lower than suggested by the colors. The red colors of the lens galaxy, $R - I = 1.13$ and $V - R = 1.46$, suggest that it is

an early-type galaxy at $z \sim 0.5$ (Fukugita et al. 1995). For SDSS J1349+1227, luminosity profile indicates that it might be a late-type galaxy, which may cause the discrepancy. For comparison we also list redshifts estimated by matching $R - I$ color of the lens galaxies to the Coleman, Wu, & Weedman (1980) early-type galaxy template. The results are fairly consistent with the estimates from the Faber–Jackson relation except for SDSS J1455+1447, where the disagreement would be solved if observed R-band magnitude were ~ 0.5 brighter. We did not pursue these discrepancies further because the image quality is not adequate for a detailed investigation. In Table 6 we list the predicted time delays using the Faber–Jackson redshift estimates from Table 7 and the measured redshift for SDSS J1620+1203.

5. Summary

As part of the SQLS project we discovered eight new gravitationally lensed quasars: SDSS J0904+1512, SDSS J1054+2733, SDSS J1055+4628, SDSS J1131+1915, SDSS J1304+2001, SDSS J1349+1227, SDSS J1455+1447, and SDSS J1620+1203. All eight lenses are two-image quasar lenses produced by galaxy-scale lens potentials. They were confirmed to be lenses by imaging and spectroscopic observations using the UH88 and Subaru telescopes. Simple mass models also suggest that the observed image configurations and fluxes are reasonable for lens systems. For SDSS J1620+1203, the redshift of the lens galaxy was determined from the absorption lines in the spectrum of the fainter quasar. The system configuration is summarized in Table 4.

Adding the eight systems reported in this paper, the SQLS has discovered 36 quasar lenses and rediscovered 11 known lenses. Among the eight new lenses, SDSS J1055+4628 will be included in the DR5 statistical lens catalog (N. Inada et al. 2010, in preparation), and SDSS J1455+1447 and SDSS J1620+1203 will be in the final DR7 statistical lens catalog of the SQLS (N. Inada et al. 2010, in preparation).

A.   LENS REDSHIFT OF SDSS J0746+4403

We also measured the lens redshift of SDSS J0746+4403 (Inada et al. 2007), one of the lensed quasars included in our statistical lens sample, using the Subaru telescope. We obtained a deep (total 2700 s exposure) spectrum of this lens with FOCAS on 21st January 2007. We used the 300B grism, the SY47 filter and a $1''\!.0$-width slit aligned along the A and B lensed images. The data were binned 2×2 on-chip. The seeing was less than $1''\!.0$ during the exposure. The two-dimensional spectrum of the system is shown in the left panel of Figure 4. In order to minimize the influence of the lensed images, we extracted a one-dimensional spectrum between the peaks of lensed images A and B (see Figure 4), using standard IRAF tasks. Although there remains some contamination from the lensed quasar images, we can clearly see galactic absorption lines of the lensing galaxy. The lens redshift is measured to be $z_l = 0.513$ from the redshifted Ca II H&K and G-band absorption lines at about 5950Å, 6000Å, and 6500Å, respectively.

REFERENCES

Abazajian, K. N., et al. 2009, ApJS, 182, 543

Blanton, M. R., Lin, H., Lupton, R. H., Maley, F. M., Young, N., Zehavi, I., & Loveday, J. 2003, AJ, 125, 2276

Blanton, M. R., Eisenstein, D., Hogg, D. W., Schlegel, D. J., & Brinkmann, J. 2005, ApJ, 629, 143

Browne, I. W. A., et al. 2003, MNRAS, 341, 13

Chae, K.-H. 2008, MNRAS, 402, 2031

Choi, Y.-Y., Park, C., & Vogeley, M. S. 2007, ApJ, 658, 884

Coleman, G. D., Wu, C.-C., & Weedman, D. W. 1980, ApJS, 43, 393

Fukugita, M., Ichikawa, T., Gunn, J. E., Doi, M., Shimasaku, K., & Schneider, D. P. 1996, AJ, 111, 1748

Fukugita, M., Shimasaku, K., & Ichikawa, T. 1995, PASP, 107, 945

Gunn, J. E., et al. 1998, AJ, 116, 3040

Gunn, J. E., et al. 2006, AJ, 131, 2332

Hennawi, J.F., et al. 2006, AJ, 131, 1

Hogg, D. W., Finkbeiner, D. P., Schlegel, D. J., & Gunn, J. E. 2001, AJ, 122, 2129

Inada, N., et al. 2007, AJ, 133, 206

Inada, N., et al. 2008, AJ, 135, 496

Inada, N., et al. 2009a, AJ, 137, 4118

Inada, N., et al. 2009b, in preparation

Ivezić, Ž., et al. 2004, Astron. Nachr, 325, 583

Kashikawa, N., et al. 2002, PASJ, 54, 819

Kochanek, C.S., 2006, in Gravitational Lensing: Strong Weak and Micro, Saas-Fee Advanced Course 33, G. Meylan, P. North, P. Jetzer, eds., (Springer: Berlin) 91

Lupton, R., Gunn, J. E., Ivezić, Z., Knapp, G. R., Kent, S., & Yasuda, N. 2001, in ASP Conf. Ser. 238, Astronomical Data Analysis Software and Systems X, ed. F. R. Harnden, Jr., F. A. Primini, and H. E. Payne (San Francisco: ASP), 269

Lupton, R. H., Gunn, J. E., & Szalay, A. S. 1999, AJ, 118, 1406

Matsumoto, A. & Futamase, T. 2008, MNRAS, 384, 843

Myers, S. T., et al. 2003, MNRAS, 341, 1

Oguri, M., et al. 2006, AJ, 132, 999

Oguri, M., et al. 2008a, AJ, 135, 512

Oguri, M., et al. 2008b, MNRAS, 391, 1973

Peng, C. Y., Ho, L. C., Impey, C. D., & Rix, H.-W. 2002, AJ, 124, 266

Pier, J. R., Munn, J. A., Hindsley, R. B., Hennessy, G. S., Kent, S. M., Lupton, R. H., & Ivezić, Ź. 2003, AJ, 125, 1559

Richards, G. T., et al. 2002, AJ, 123, 2945

Rusin, D., et al. 2003, ApJ, 587, 143

Schneider, D. P., et al. 2007, AJ, 134, 102

Schneider, D. P., et al. 2009, in preparation

Schneider, P., Kochanek, C.S., & Wambsganss, J. 2006, in Gravitational Lensing: Strong, Weak and Micro, Saas-Fee Advanced Course 33, G. Meylan, P. North, P. Jetzer, eds., (Springer: Berlin)

Smith, A., et al. 2002, AJ, 123, 2121

Stoughton, C., et al. 2002, AJ, 123, 485

Tucker, D. L., et al. 2006, Astron. Nachr, 327, 821

Wisotzki, L., Koehler, T., Kayser, R., Reimers, D. 1993, A&A, 278, L15

York, D. G., et al. 2000, AJ, 120, 1579
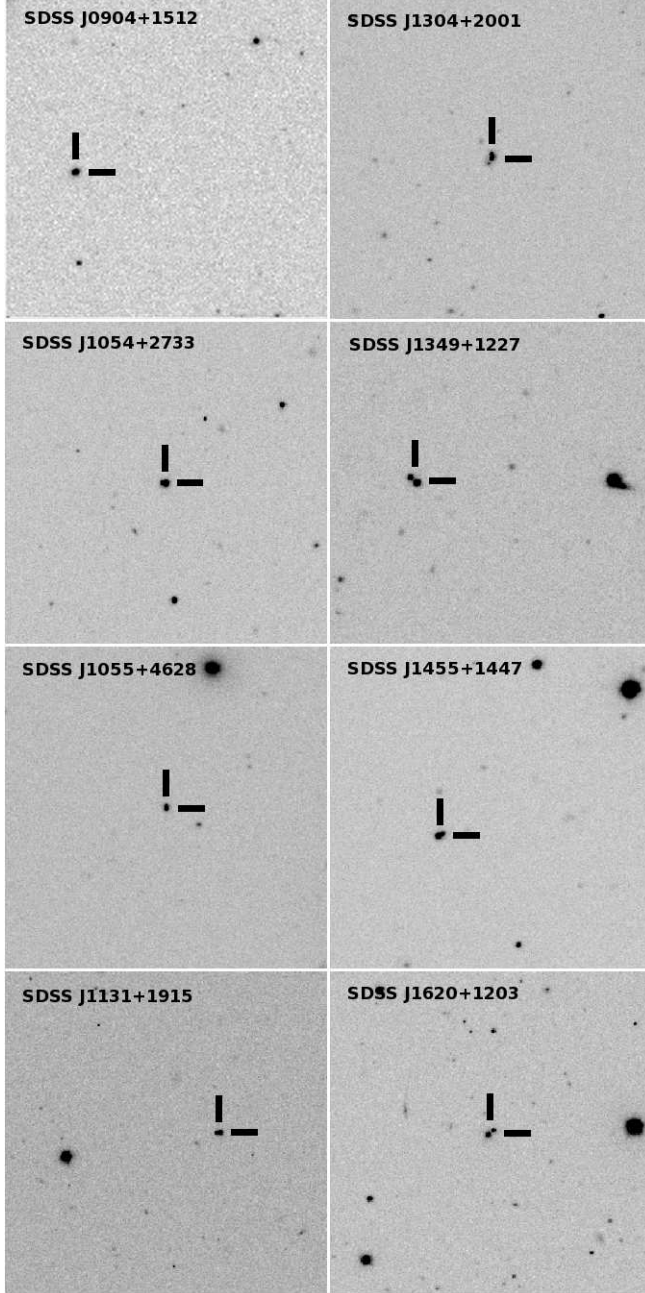
Fig. 1.— SDSS i-band images of the eight lens systems. The size of each image is $2' \times 2'$, and north is up and east is left.
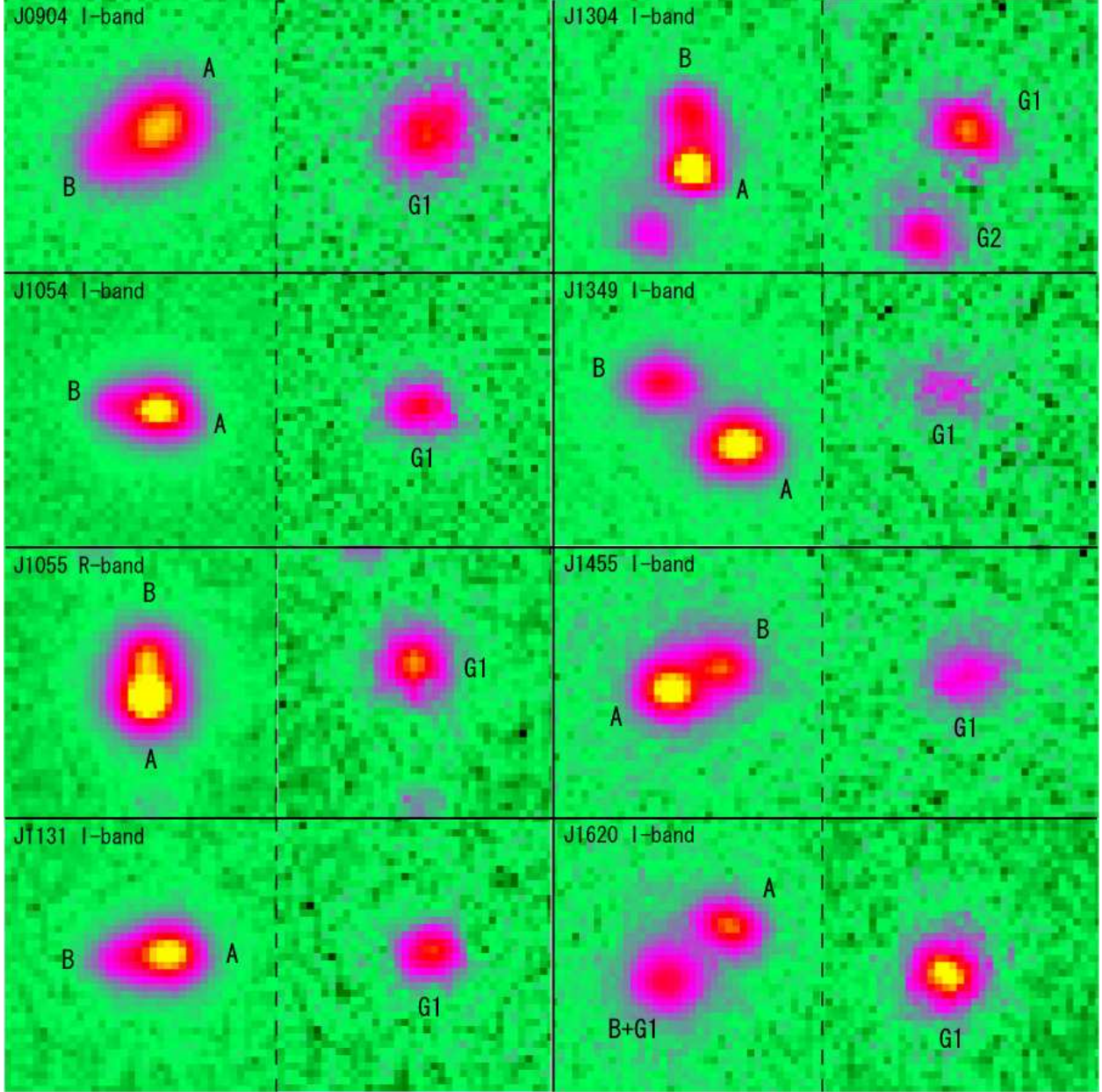
Fig. 2.— Images taken by the UH88 and Subaru telescopes (left panels of each) and the residuals after fitting and subtracting two PSFs using GALFIT (right panels of each). The residual objects labeled by "G1" or "G2" are the lens galaxies. These are Tek2k I-band images except for SDSS J0904+1512 (I band, OPTIC) and SDSS J1055+4628 (R band, FOCAS). The size of the images is approximately $8'' \times 8''$, and north is up and east is left.
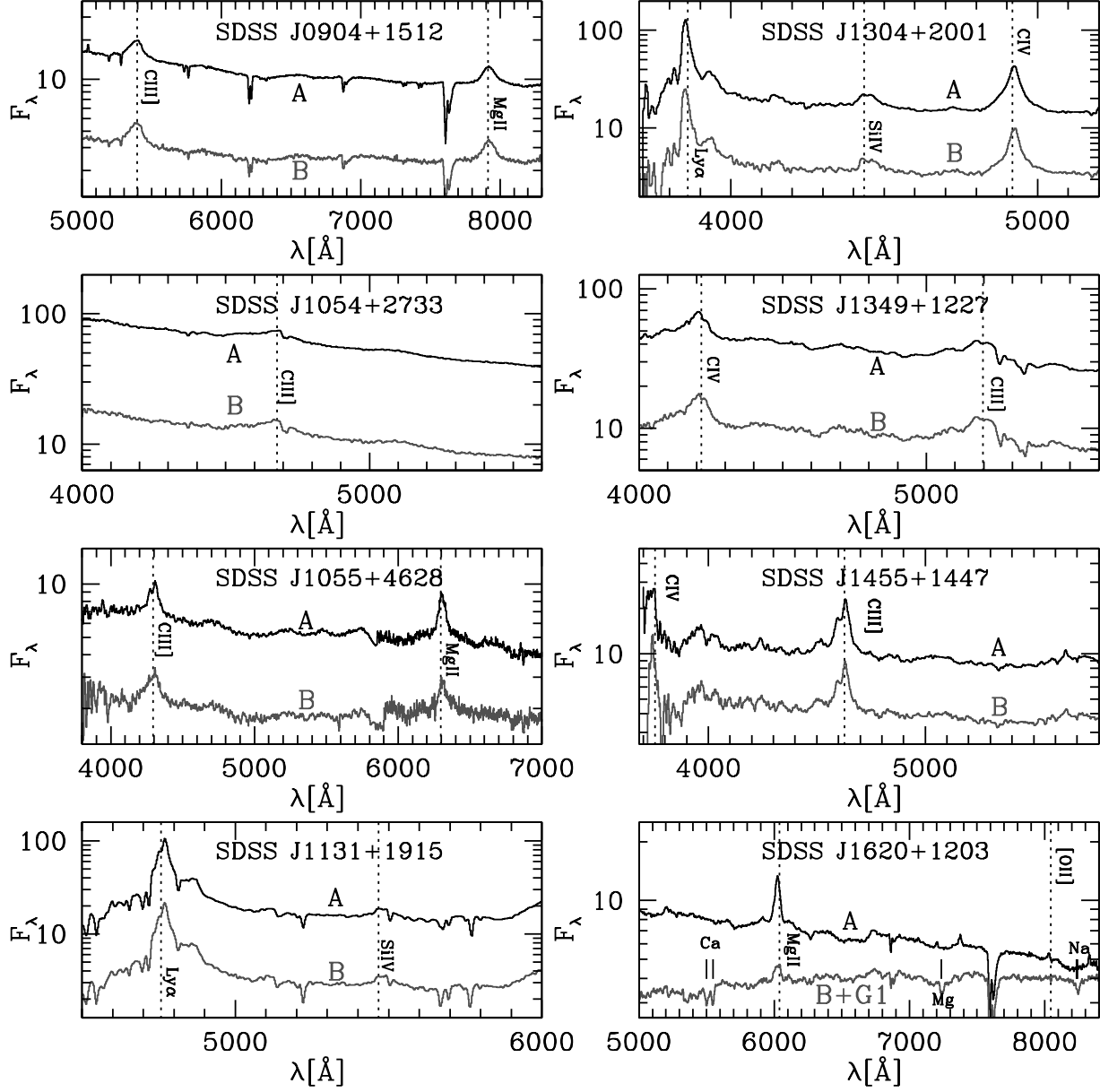
Fig. 3.— FOCAS spectra of the eight lens systems. The flux density units are $10^{-17} \mathrm{erg} \, \mathrm{cm}^{-2} \mathrm{s}^{-1} \mathring{A}^{-1}$. For SDSS J1055+4628, two exposures were merged at $\sim 5850 \mathring{A}$. Absorption lines from the lens galaxy are observed in the spectrum of the fainter image of SDSS J1620+1203. Absorption lines by some intervening systems are also observed in SDSS J0904+1512 (Mg II and Fe II at $z = 1.2168 \pm 0.0002$), SDSS J1054+2733 (Mg II and Fe II at $z = 0.6794 \pm 0.0002$), SDSS J1131+1915 (Fe II at $z = 1.1890 \pm 0.0005$ and a DLA at $z = 2.6025 \pm 0.0002$ with Si II, O I, and C II), and SDSS J1349+1227 (Fe II at $z = 1.2347 \pm 0.0002$ and $z = 1.2385 \pm 0.0002$). The features at $\sim 6900 \mathring{A}$ and $\sim 7600 \mathring{A}$ are telluric.
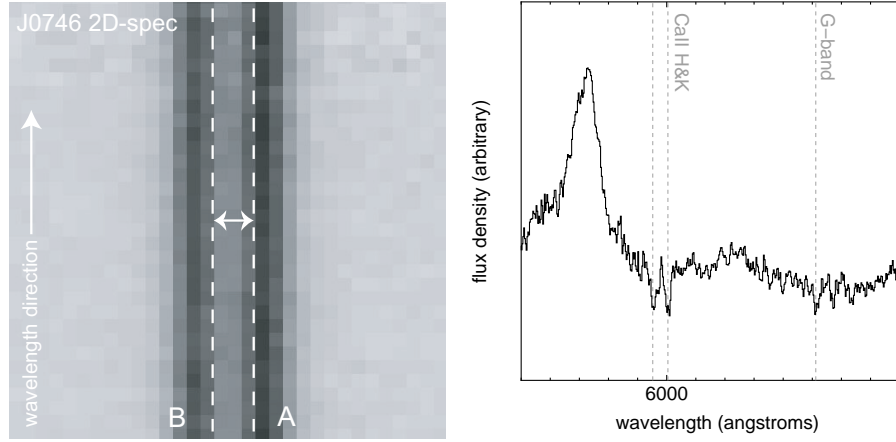
Fig. 4.— Section of the two-dimensional FOCAS spectrum (*left*) of SDSS J0746+4403 (Inada et al. 2007) and the one-dimensional spectrum (*right*) extracted from the central region shown in the left panel, denoted by the two dashed lines. We can clearly see the Ca II H&K and *G*-band absorption lines from the lens galaxy at $z_l = 0.513$, in the right panel.

Table 1.   SDSS Properties of the Lens Systems

| Object	R.A.(J2000)	Decl.(J2000)	u	g	r	i	z	redshift
SDSS J0904+1512	09:04:04.15	+15:12:54.5	17.93±0.02	17.77±0.02	17.80±0.01	17.58±0.01	17.54±0.02	1.826±0.002
SDSS J1054+2733	10:54:40.83	+27:33:06.4	17.16±0.02	16.93±0.02	16.95±0.02	16.84±0.02	16.89±0.02	1.452±0.002
SDSS J1055+4628	10:55:45.45	+46:28:39.4	19.38±0.04	19.28±0.02	18.79±0.03	18.78±0.02	18.79±0.04	1.249±0.001
SDSS J1131+1915	11:31:57.72	+19:15:27.7	19.90±0.04	18.23±0.02	18.00±0.02	18.04±0.04	17.85±0.03	2.915±0.001
SDSS J1304+2001	13:04:43.58	+20:01:04.2	18.93±0.02	18.66±0.02	18.70±0.03	18.49±0.03	18.33±0.03	2.175±0.002
	13:04:43.60	+20:01:05.8	21.08±0.32	20.45±0.35	19.98±0.19	19.93±0.23	19.44±0.12	$\cdots$
SDSS J1349+1227	13:49:29.84	+12:27:06.8	17.99±0.02	17.85±0.02	17.79±0.02	17.51±0.03	17.53±0.03	1.722±0.002
	13:49:30.00	+12:27:08.7	19.70±0.22	19.32±0.17	19.11±0.12	18.73±0.13	18.62±0.13	$\cdots$
SDSS J1455+1447	14:55:01.91	+14:47:34.8	19.53±0.03	19.11±0.02	18.61±0.01	18.30±0.02	18.04±0.03	1.424±0.001
SDSS J1620+1203	16:20:26.14	+12:03:42.0	19.82±0.04	19.70±0.03	19.26±0.04	19.21±0.05	19.23±0.09	1.158±0.002
	16:20:26.27	+12:03:40.3	21.30±0.13	20.76±0.12	19.90±0.08	19.52±0.06	19.23±0.07	$\cdots$

Note.   — Magnitudes are PSF magnitudes without Galactic extinction corrections.   The two images of SDSS J1304+2001 and SDSS J1349+1227 are split by the SDSS pipeline. The fainter quasar in SDSS J1620+1203 is overlapped by the bright lens galaxy and classified as a galaxy by the SDSS software.

Table 2.   Imaging Observations

Object	Imager	Date of Observation (UT)	Exposure Time (sec)
SDSS J0904+1512	Tek2k(VR), OPTIC(I)	12/Apr/07(V), 20/Jan/09(R), 4/May/06(I)	300(V), 600(R), 800(I)
SDSS J1054+2733	Tek2k(VRI)	12/Apr/07(VR), 16/Nov/06(I)	300(V), 200(R), 600(I)
SDSS J1055+4628	UH8k(V), Tek2k(BI), FOCAS(R)	13/Nov/07(B), 18/Nov/04(V), 1/Feb/09(R), 12/Nov/07(I)	400(B), 360(V), 120(R), 400(I)
SDSS J1131+1915	Tek2k(VIz')	12/Apr/07(V), 16/Apr/07(Iz')	300(V), 800(I), 800(z')
SDSS J1304+2001	Tek2k(VRI)	7/Mar/08(VRI)	400(V), 400(R), 400(I)
SDSS J1349+1227	Tek2k(VRI), QUIRC(H)	16/Apr/09(VRI), 22/Feb/05(H)	400(V), 400(R), 400(I), 1080(H)
SDSS J1455+1447	Tek2k(VRI)	16/Apr/09(VRI)	300(V), 300(R), 400(I)
SDSS J1620+1203	Tek2k(VRI)	16/Apr/09(VRI)	400(V), 300(R), 300(I)

Note. — Date of observation is the UT date when the exposures were started.

Table 3.   FOCAS Spectroscopic Observations

Object	slit width	grism	filter	wavelength coverage (Å)	R	Date of Observation (UT)	Exposure time (sec)
SDSS J0904+1512	$1''$	300B	SY47	4700-9100	400	23/Jan/07	1000
SDSS J1054+2733	$1''$	300B	L600	3700-6000	400	1/Feb/09	480
SDSS J1055+4628 (red)	$0.8''$	300R	SO58	5800-10000	500	7/May/08	300
SDSS J1055+4628 (blue)	$1''$	300B	L600	3700-6000	400	1/Feb/09	720
SDSS J1131+1915	$1''$	300B	L600	3700-6000	400	1/Feb/09	720
SDSS J1304+2001	$1''$	300B	L600	3700-6000	400	1/Feb/09	720
SDSS J1349+1227	$1''$	300B	L600	3700-6000	400	1/Feb/09	480
SDSS J1455+1447	$1''$	300B	L600	3700-6000	400	1/Feb/09	480
SDSS J1620+1203	$1''$	300B	SY47	4700-9100	400	1/Feb/09	720

Table 4.   Relative Astrometry and Absolute Photometry of Lens Systems

Component	Δ X (arcsec)	Δ Y (arcsec)	V	R	I
SDSS J0904+1512 ($\theta = 1\rlap{.}''128 \pm 0\rlap{.}''007$)					
A	0.000±0.003	0.000±0.003	18.18±0.01	17.88±0.01	17.71±0.04
B	−0.988±0.007	−0.544±0.004	20.15±0.02	19.89±0.04	19.13±0.02
G1	−0.217±0.033	−0.091±0.018	21.19±0.12	19.73±0.07	18.60±0.07
SDSS J1054+2733 ($\theta = 1\rlap{.}''269 \pm 0\rlap{.}''004$)					
A	0.000±0.002	0.000±0.002	17.21±0.01	17.09±0.01	16.94±0.01
B	−1.260±0.004	0.149±0.004	19.22±0.01	18.98±0.01	18.82±0.02
G1	−0.391±0.042	−0.048±0.018	$\cdots$	19.13±0.03	18.75±0.05
SDSS J1055+4628 ($\theta = 1\rlap{.}''146 \pm 0\rlap{.}''004$)					
A	0.000±0.002	0.000±0.002	20.02±0.01	19.17±0.01	18.98±0.01
B	−0.024±0.013	1.146±0.004	21.07±0.01	20.67±0.03	20.17±0.04
G1	−0.136±0.033	0.871±0.040	$\cdots$	20.60±0.10	19.73±0.05
SDSS J1131+1915 ($\theta = 1\rlap{.}''462 \pm 0\rlap{.}''007$)					
A	0.000±0.002	0.000±0.002	18.51±0.01	$\cdots$	17.91±0.02
B	−1.455±0.007	−0.145±0.004	20.53±0.02	$\cdots$	19.62±0.02
G1	−0.378±0.079	−0.013±0.020	$\cdots$	$\cdots$	19.45±0.07
SDSS J1304+2001 ($\theta = 1\rlap{.}''865 \pm 0\rlap{.}''004$)					
A	0.000±0.002	0.000±0.002	18.70±0.01	18.54 ± 0.01	18.05±0.01
B	-0.116±0.004	1.861±0.004	20.23±0.01	20.04 ± 0.01	19.61±0.02
G1	0.092±0.009	1.225±0.015	20.68±0.16	19.71 ± 0.01	18.74±0.08
G2	-1.245±0.009	-1.951±0.007	20.42±0.14	19.58 ± 0.23	18.96±0.17
SDSS J1349+1227 ($\theta = 3\rlap{.}''002 \pm 0\rlap{.}''004$)					
A	0.000±0.002	0.000±0.002	17.79±0.01	17.59±0.01	17.14±0.01
B	−2.335±0.004	1.886±0.004	19.30±0.01	19.01±0.01	18.49±0.01
G1	−2.105±0.048	1.727±0.037	20.99±0.09	20.71±0.06	19.35±0.05
SDSS J1455+1447 ($\theta = 1\rlap{.}''727 \pm 0\rlap{.}''004$)					
A	0.000±0.002	0.000±0.002	19.50±0.02	18.83±0.01	18.25±0.01
B	1.578±0.004	0.702±0.004	20.30±0.02	19.83±0.02	19.00±0.01
G1	0.591±0.031	0.400±0.015	20.29±0.08	19.62±0.03	18.51±0.07
SDSS J1620+1203 ($\theta = 2\rlap{.}''765 \pm 0\rlap{.}''011$)					
A	0.000±0.004	0.000±0.002	20.07±0.01	19.12±0.01	18.64±0.01
B	−2.080±0.011	−1.822±0.011	21.30±0.07	20.73±0.10	19.94±0.05
G1	−1.756±0.013	−1.449±0.013	20.10±1.16	18.49±0.29	17.59±0.45

Note. — Positions of each component were derived from the I-band images, except for the R-band image used for SDSS J1055+4628. The positive directions of X and Y are west

and north, respectively. SDSS J1131+1915 was not observed in the R-band. The V-band fluxes of the lens galaxies of SDSS J1054+2733, SDSS J1055+4628, and SDSS J1131+1915 are too faint to be measured. The errors on the positions and fluxes include only statistical errors reported by GALFIT. The errors on the image separation were calculated on the assumption that the position uncertainties are all uncorrelated.

Table 5.   Luminosity Profile of Lens Galaxies

Object	$r_e{}^{\mathrm{a}}$ ($''$)	n^{b}	e^{c}	$\theta_e{}^{\mathrm{d}}$ (deg)
SDSS J0904+1512	0.26 ± 0.03	4.11 ± 1.04	0.49 ± 0.04	-20 ± 5
SDSS J1054+2733	0.42 ± 0.04	3.67 ± 0.75	0.42 ± 0.04	-88 ± 5
SDSS J1055+4628	0.53 ± 0.05	5.42 ± 1.53	0.07 ± 0.04	$+28 \pm 22$
SDSS J1131+1915	0.14 ± 0.04	2.38 ± 1.22	0.82 ± 0.82	-15 ± 11
SDSS J1304+2001	0.54 ± 0.02	2.90 ± 0.45	0.42 ± 0.03	$+58 \pm 4$
SDSS J1349+1227	1.06 ± 0.13	1.69 ± 0.52	0.24 ± 0.06	$+71 \pm 11$
SDSS J1455+1447	1.49 ± 0.20	3.50 ± 0.54	0.28 ± 0.04	-76 ± 5
SDSS J1620+1203	3.70 ± 3.20	6.62 ± 2.53	0.25 ± 0.03	-21 ± 4

Note. — Sérsic parameters measured in the I band images (R band for SDSS J1055+4628) using GALFIT.

[a]Effective radius of the Sérsic profile.

[b]Sérsic index.

[c]Ellipticity.

[d]Major axis position angle measured east of north.

Table 6.   Mass Models of Lenses

Object	$R_{\mathrm{Ein}}('')$	e	$\theta_e(\deg)$	μ_{tot}[a]	Δt [b] (day)
SDSS J0904+1512	0.529 ± 0.007	0.72 ± 0.05	$+31 \pm 2$	6.9 ± 1.0	9.1 ± 0.6
SDSS J1054+2733	0.598 ± 0.004	0.52 ± 0.06	-14 ± 1	12.7 ± 2.2	10.1 ± 1.2
SDSS J1055+4628	0.600 ± 0.016	0.37 ± 0.08	-49 ± 7	3.4 ± 0.5	23.4 ± 2.2
SDSS J1131+1915	0.680 ± 0.006	0.58 ± 0.09	$+5 \pm 1$	10.2 ± 1.9	22.4 ± 3.3
SDSS J1304+2001	0.987 ± 0.008	0.23 ± 0.02	$+27 \pm 3$	7.9 ± 0.8	24.0 ± 0.9
SDSS J1349+1227	1.399 ± 0.010	0.57 ± 0.09	-42 ± 4	2.0 ± 0.1	450.1 ± 8.8
SDSS J1455+1447	0.853 ± 0.004	0.16 ± 0.03	$+10 \pm 2$	12.7 ± 2.0	11.0 ± 1.4
SDSS J1620+1203	1.353 ± 0.021	0.23 ± 0.06	$+21 \pm 10$	2.8 ± 0.1	179.3 ± 2.0

Note. — Errors are estimated from 1000 random data for each system with scatter in Table 4 for positions and 0.2 mag for image magnitudes. We used the redshifts estimated by the Faber–Jackson relation in Table 7 to compute the predicted time delays, or the measured redshift for SDSS J1620+1203. We do not include the uncertainty of the redshift for the error estimate.

[a]Total magnification.

[b]Time delay.

Table 7.   Predicted Redshifts and Apparent V and R Magnitudes of Lens Galaxies

Object	V	R	Redshift (FJ)	Redshift $(R - I)$
SDSS J0904+1512	20.1 (21.2)	19.1 (19.7)	0.19	0.54
SDSS J1054+2733	20.3 $(\cdots)$	19.3 (19.1)	0.23	_[b]
SDSS J1055+4628	21.6 $(\cdots)$	20.5 (20.6)	0.39	0.38
SDSS J1131+1915	21.2 $(\cdots)$	20.1 $(\cdots)$	0.32	$\cdots$
SDSS J1304+2001	20.5 (20.4)	19.3 (19.6)	0.32	0.46
SDSS J1349+1227	21.7 (21.0)	20.3 (20.7)	0.63	0.66
SDSS J1455+1447	20.2 (20.3)	19.0 (19.6)	0.27	0.53
SDSS J1620+1203	20.2 (20.1)	18.9 (18.5)	0.398[a]	0.41

Note. — Values in parenthesis are the observed magnitude in Table 4. The typical uncertainties of redshift (FJ) and redshift $(R - I)$ are ~ 0.1, considering 0.5 mag and 0.1 mag scatter for luminosity and color of galaxies, respectively.

[a]Redshift of SDSS J1620+1203 is measured spectroscopically and I-band magnitude is estimated to be 18.3 at this redshift. FJ estimate will be 0.27 to recover the observed I-band magnitude of 17.59.

[b]$R - I$ color is too blue to match the template.